

Cross-Track Infrared Sounder Spectral Gap Filling Toward Improving Intercalibration Uncertainties

Hui Xu^{ID}, Yong Chen^{ID}, and Likun Wang

Abstract—The cross-track infrared sounder (CrIS) is a hyper-spectral infrared sounder with 2211 (full-spectral resolution) channels over three wavelength ranges. Due to its excellent calibration and high spectral resolution, CrIS radiances are also used as an infrared reference to check calibration accuracy of other narrow- or broadband instruments. However, there are spectral gaps between the CrIS bands, which impact the accuracy of intercomparison between CrIS and other instruments. To fill up the spectral gaps, this paper develops a new method to predict the CrIS gap channels. A training data set was first built based on the spectra selected from different seasons to represent different atmospheric and surface conditions. The principal component regression method is then developed to derive the prediction coefficients between the CrIS measured and the gap channel spectra. The prediction accuracies are around $0.005\text{ K} \pm 0.18\text{ mK}$, $0.06\text{ K} \pm 0.45\text{ mK}$, and $0.05\text{ K} \pm 0.71\text{ mK}$ for the long-, middle-, and short-wave gap channels, respectively. It should note that the predicted channels are intended to be only used in the intercomparison purposes instead of providing exact information of these gap channels. When comparing the CrIS gap radiances with atmospheric infrared sounder and infrared atmospheric sounding interferometer, consistent results are observed between CrIS and other sounders. The further intercomparison results with visible infrared imaging radiometer suite and advanced baseline imager suggest that the predicted gap radiances are good enough for the intercalibration purposes and this method can be confidently applied in global space-based intercalibration system community.

Index Terms—Cross-track infrared sounder (CrIS), intercalibration, principal component regression (PCR), spectrum gap filling.

I. INTRODUCTION

THE cross-track infrared sounder (CrIS), a hyper-spectral infrared sounder flying on the afternoon orbit Suomi National Polar-orbiting Partnership (SNPP), and Joint Polar Satellite System (JPSS) satellite, was developed for providing atmospheric temperature and moisture sounding information for weather and climate applications [1]. Indeed, CrIS data have been widely used in numerical weather prediction and

Manuscript received February 7, 2018; revised April 21, 2018 and May 25, 2018; accepted July 10, 2018. Date of publication August 9, 2018; date of current version December 24, 2018. This work was supported by the National Oceanic and Atmospheric Administration under Grant NA14NES4320003 (Cooperative Institute for Climate and Satellites: Cooperative Agreement 2014–2019) at the University of Maryland/ESSIC. (*Corresponding author: Hui Xu*)

The authors are with the Earth System Science Interdisciplinary Research Center, University of Maryland, College Park, MD 20740 USA (e-mail: huixu@umd.edu; Yong.Chen@noaa.gov; Likun.Wang@noaa.gov).

Color versions of one or more of the figures in this paper are available online at <http://ieeexplore.ieee.org>.

Digital Object Identifier 10.1109/TGRS.2018.2857833

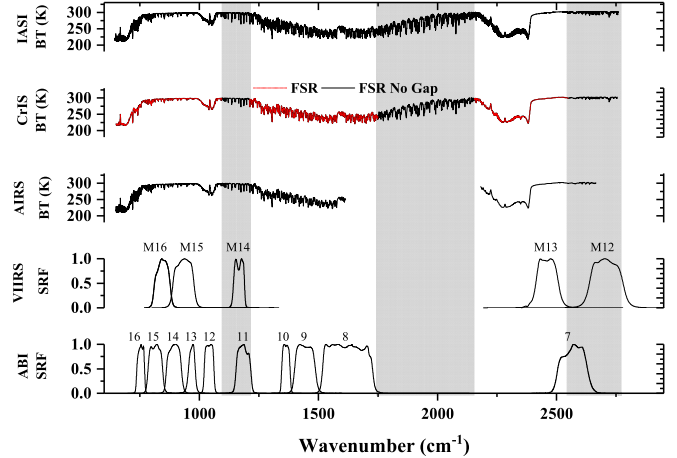


Fig. 1. LBLRTM simulated spectra of IASI, AIRS, and CrIS along with the channel response of VIIRS and ABI. The shadow areas show the spectral regions where CrIS do not measure.

retrievals of atmospheric profiles, trace gases, and land surface and cloud properties [2]–[4]. Due to its high-quality calibration accuracy as well as hyper-spectral nature [5], CrIS spectral radiances also routinely serve as an infrared reference to check calibration accuracy of other broad- or narrow-band instruments, such as advanced baseline imager (ABI) on Geostationary Operational Environmental Satellite (GOES) 16, visible infrared imaging radiometer suite (VIIRS) on SNPP [6]–[8], and advanced Himawari imager (AHI) on HIMAWARI (the daily intercalibration between AHI and CrIS can be found in Japan Meteorological Agency's website <http://www.data.jma.go.jp/mscweb/data/monitoring/calibration.html>) and other instruments under the global space-based intercalibration system (GSICS) framework.

By design, CrIS spectra are separated into three bands: long-wave (LW) band at $650\text{--}1095\text{ cm}^{-1}$, middle-wave (MW) band at $1210\text{--}1750\text{ cm}^{-1}$, and short-wave band (SW) at $2155\text{--}2550\text{ cm}^{-1}$, as illustrated in Fig. 1. Two spectral gaps—one from $1095\text{ to }1210\text{ cm}^{-1}$ and the other from $1750\text{ to }2155\text{ cm}^{-1}$ —exist between these bands. The spectral gaps will also exist in the upcoming JPSS-1 and future JPSS-2 CrIS in the next decade. These spectral gaps may not significantly impact on weather-related applications (including data assimilations and geophysical parameter retrieval). However, for the intercalibration applications that use CrIS data to evaluate the performance of other instruments, these spectral gaps limit the intercalibration accuracy for the bands that are

TABLE I
CRIS SPECTRAL BAND COVERAGE FOR BROADBAND
INSTRUMENT USED IN THIS PAPER

Sensors	Channel number	Central wavenumber (cm^{-1})	SRF covered by CrIS spectrum with gap
ABI on GOES-16	7	2570.37	32.90%
	8	1620.53	99.78%
	11	1184.22	10.70%
VIIRS on S-NPP	M14	1165.96	0.01%

The spectral coverage is calculated by dividing the total channel Spectral Response Function (SRF) with that of covered only by CrIS spectrum. Only the channels that are not fully covered by CrIS are listed.

not fully covered by the CrIS spectra (e.g., VIIRS M14, and ABI channel 11 in Table I and Fig. 1). In addition, it is desirable to extend CrIS spectra beyond 2550 cm^{-1} , which then can be compared to instruments with some SW channels not covered by the CrIS spectral range (e.g., ABI channel 7 in Table I and Fig. 1). Therefore, it is important to develop a method to fill the CrIS gap channels from the measured CrIS spectra, making the CrIS intercalibration results comparable with other hyper-spectral sounders, such as the atmospheric infrared sounder (AIRS) and infrared atmospheric sounding interferometer (IASI).

Several spectral gap-filling methods for hyper-spectral infrared sounders have been developed for intercalibration purposes in previous studies. In 2006, Tobin *et al.* [9] pioneered in the development of the first gap-filling method when intercalibrating AIRS and moderate resolution imaging spectroradiometer (MODIS). In their study, the so-called “convolution corrections” were simulated from the U.S. standard atmosphere to correct the error caused by AIRS spectral gaps. The same method also has been applied to long-term assessment of Aqua MODIS radiance observation using comparisons with AIRS and IASI [10]. Gunshor *et al.* [11] further applied the similar method to the intercomparison of AIRS with GOES imagers. In 2009, Tahara and Kato [12] developed the spectral gap compensation method which was widely used under the GSICS framework. In their study, the spectral gaps of the hyper-spectral infrared sounders are calculated by regression analysis using radiative transfer simulated radiances with respect to the eight atmospheric model profiles as explanatory variables. These methods work effectively for small spectral gaps (like AIRS) and indeed make significant improvement on the accuracy of intercalibration results. However, it is very challenging for large CrIS spectral gaps [as shown in Fig. 1] because: 1) big gaps are less well constrained by using abovementioned methods and 2) the atmospheric, cloud, and surface conditions vary temporally and locally, and thus only relying on several static spectra is not good enough to predict the CrIS gap radiances.

To meet this challenge, it is essential to establish a reliable relationship between the CrIS measured and gap channels [13]. However, due to radiance correlations among different channels, it is not straightforward to establish the relationship through a conventional regression method. The fitting results between the measured (predictors) and the gap

(response variables) channel radiances will become unstable and far from the truth because they are highly collinear in the equation system. On the other hand, the principal component regression (PCR) is an optimized regression analysis technique that is based on principal component analysis (PCA) for analyzing multiple regression data that suffer from multicollinearity [14], [15]. The orthogonal transformation procedure of the PCA converts correlated variables into a set of linearly uncorrelated principal components that describe the variances of the original data set. In addition, it can transform most of the effective signals into a few leading principal components and the noise into the rest of the principal components [16]. By only using the leading principal components as predictors instead of all the dependent explanatory variables, one can also greatly reduce the dimension and instrument noise from the measurements. Therefore, this paper develops a PCR based spectral gap prediction method to fill up the CrIS unmeasured channels. The purpose is to improve the CrIS spectral coverage for intercalibration applications by filling up the spectral gaps with the information contained in the CrIS measurements.

This paper is organized as follows. Section II describes the methodology of the CrIS gap channel prediction. Section III presents a comprehensive evaluation on the accuracy of the predicted CrIS gap channels. Section IV demonstrates the performance and benefits of the predicted CrIS gap channels in intercomparison between CrIS and broadband instruments. The discussions and conclusions are given in Section V.

II. DATA AND METHODS

A. Data Product

CrIS is a Michelson interferometer onboard the Suomi NPP spacecraft at a nominal altitude of 824 km in a sun-synchronous orbit with local equatorial crossing times of 13:30 (ascending) and 01:30 (descending). It measures the spectrum in three infrared (IR) bands simultaneously as described in Section I. For each scan, CrIS collects 30 earth and four embedded space and blackbody calibration targets field of regards (FORs) by a 3×3 detector array. It provides a total of 1305 radiance channels in the normal spectral resolution (NSR) of 0.625 , 1.25 , and 2.5 cm^{-1} for LW, MW, and SW bands, respectively. CrIS can also be operated in a full-spectral resolution (FSR) mode of 0.625 cm^{-1} with 2211 channels over the three bands [17].

In this paper, the FSR CrIS radiance data are used. In addition, the IASI level 1C (hereafter, IASI/A, and IASI/B are referred to IASI on MetOp-A and MetOp-B, respectively), AIRS level 1C, ABI level 1B, and VIIRS SDR radiance products are also used. Particularly, the AIRS level 1C data is generated from AIRS level 1B and the bad channels and small gaps in level 1B data are corrected and filled by the level 1C algorithm. Detailed information of these satellite products can be found in previous studies and their corresponding technical reports [18]–[23].

B. Methodology

This paper introduces a new gap channel prediction method based on spectral information derived from CrIS current

three bands. Fundamentally, the atmospheric spectrum is determined by the atmospheric temperature and humidity conditions, trace gas concentration, and land and cloud conditions. The basic assumption of the proposed gap-filling method is that the CrIS gap channel information contents have already existed in current measured channels. Using the spectral gap 1095.625–1209.375 cm⁻¹ at atmospheric window region as an example, their spectral information is strongly correlated with the CrIS measured spectra from 800 to 1000 cm⁻¹. The same correlation also applies to water vapor regions from 1750.625 to 2154.375 cm⁻¹, which could possibly be predicated by the channels from 1250 to 1750 cm⁻¹. The spectral absorption of some trace gases, such as N₂O and CH₄, also happens at both the CrIS measured and gap channels. Therefore, the CrIS gap channel's prediction can be simplified to establish an accurate and reliable relationship between the CrIS measured and gap channels.

1) *Training Data Set*: To establish this relationship, a data ensemble with enough samples is required, which includes both measured and gap spectra. For convenience, we hereafter refer to the CrIS full spectrum, which include both existing and gap channels as the full-CrIS spectrum. A full-CrIS spectrum has 3369 channels, including a total of 1158 gap channels, i.e., 183 channels between the LW and MW bands, 647 channels between the MW and SW bands, and 328 channels extending the SW band to 2755 cm⁻¹. One way to generate the training data set is to simulate the spectra for both existing and gap channels by using a forward radiative transfer model. However, it is very difficult to simulate spectra under different atmospheric and surface conditions with a global representation. An alternative method is to convert the IASI spectra to the full-CrIS spectra. Both CrIS and IASI are Fourier transform infrared spectrometers. The IASI spectrum has a higher spectral resolution (0.25 cm⁻¹) than that of CrIS and also covers all the CrIS measured and gap spectral channels, allowing it to be accurately converted into the full-CrIS. More importantly, CrIS and IASI generally agree well based on [24]. Five steps are performed to convert the IASI spectra to full-CrIS with an equal spectral resolution:

Apply a raised cosine bandpass filter $f(\sigma)_{\text{cos}}$ to the selected IASI spectra $R(\sigma)_{\text{IASI}}$ to restrict them to the full-CrIS desired spectral band $R(\sigma)_{\text{desired}}$

$$R(\sigma)_{\text{desired}} = f(\sigma)_{\text{cos}} \cdot R(\sigma)_{\text{IASI}}. \quad (1)$$

Convert the desired IASI spectra $R(\sigma)_{\text{desired}}$ to interferogram $I(x)_{\text{desired}}$ using inverse Fourier transform

$$I(x)_{\text{desired}} = \int_{\sigma} R(\sigma)_{\text{desired}} \cdot e^{i2\pi\sigma x} d\sigma. \quad (2)$$

Deapodize the $I(x)_{\text{desired}}$ using IASI's Gaussian apodization function $\gamma(x)_{\text{gaussian}}$ and truncating them into CrIS maximum OPD specification with a boxcar filter $f(x)_{\text{box}}$

$$I(x)_{\text{truncated}} = \frac{I(x)_{\text{desird}}}{\gamma(x)_{\text{gaussian}}} \cdot f(x)_{\text{box}}. \quad (3)$$

Apply the CrIS hamming apodization function $\gamma(x)_{\text{hamming}}$ to the truncated interferogram to get the apodized full-CrIS

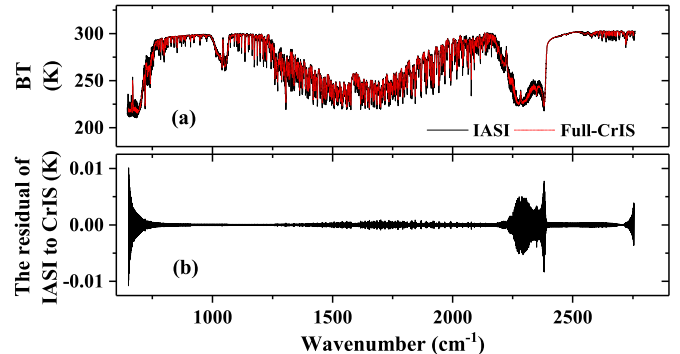


Fig. 2. (a) IASI and full-CrIS (without spectral gap) spectra in BT that simulated by LBLRTM using an identical atmospheric profile as the input. (b) BT differences of LBLRTM simulated full-CrIS minus IASI converted full-CrIS. The LBLRTM used in the simulation is version 11.1 with HITRAN 2004 database and AER updates version 2. The TOA radiances are calculated under clear sky condition from a typical tropical atmospheric profile that is contained in the LBLRTM.

interferogram $I(x)_{\text{Full-CrIS}}$

$$I(x)_{\text{full-CrIS}} = I(x)_{\text{truncated}} \cdot \gamma(x)_{\text{hamming}}. \quad (4)$$

Transform back to the spectral domain with forward Fourier transform to get the full-CrIS spectra $R(\sigma)_{\text{full-CrIS}}$ training data set

$$R(\sigma)_{\text{full-CrIS}} = \int_x I(x)_{\text{full-CrIS}} \cdot e^{-i2\pi\sigma x} dx. \quad (5)$$

To evaluate the performance of the mentioned CrIS simulation method, two spectra are simulated by line-by-line radiative transfer model (LBLRTM) using an identical atmospheric profile as input, as shown in Fig. 2. One spectrum is first simulated at IASI's spectral specification [black line in Fig. 2(a)], and then converted into full-CrIS resolution using above method. The other one is directly sampled at the spectral grid of full-CrIS [red line in Fig. 2(a)] which can be regarded as the truth value. Their spectral differences are given in Fig. 2(b) in brightness temperature (BT). The conversion errors are very small, ranging from -0.01 to 0.01 K with ringing patterns, suggesting that these random errors are negligible and will be canceled out when convolving over the spectral response function (SRF) of the broadband sensors.

By using this conversion method, a large data ensemble of full-CrIS spectra covering the spectral range from 650 to 2755 cm⁻¹ with an equal spectral resolution of 0.625 cm⁻¹ is built up as the training data set based on spectral information observed from IASI/B. As a matter of fact, both IASI/A and IASI/B have been proved are accurate calibrated hyper-spectral sounders [20], [24] and can provide enough spectral information for training data set. However, since IASI/A is now out of its designed five years mission (October 2006) and potentially degraded, its newly launched successor IASI/B (September 2012) was used in this paper. The training data set is obtained from all the FOVs of the full orbit of IASI/B spectra with a scan interval of two and FOR interval of three collected in different seasons (winter: January 10, 2016, spring: April 6, 2016, summer: June 26, 2016, and autumn: November 1, 2016). Moreover, the

spectra with channel radiances less than zero are considered as invalid data with large noise and removed from the training data set. Finally, there are totally 636402 spectra was selected from the four days IASI/B measurements.

2) PCR-Based Spectral Gap Prediction: Suppose that the CrIS gap channel radiance $y \in \{y_1, y_2, \dots, y_m, m = 1158\}$ can be predicted by the measured channel radiances $x \in \{x_1, x_2, \dots, x_n, n = 2211\}$ using the following equation:

$$y_i = \beta_{0,i} + \beta_{1,i} \cdot x_1 + \beta_{2,i} \cdot x_2 + \dots + \beta_{j,i} \cdot x_j + \dots + \beta_{n,i} \cdot x_n + u_i \quad (6)$$

where $\beta_{j,i}$ is the prediction coefficients, u_i is the residual, j is the j th measured channel, and i is the i th gap channel. Thus, all the gap channel radiances with a total of t observations can be written in the matrix form

$$Y = D_X \times B + U \quad (7)$$

where Y is an $m \times t$ matrix containing the CrIS gap channel radiances (m channels and t samples), D_X is the design matrix with a dimension $(n+1) \times t$ with the first column elements set to 1 and the rest of columns containing the CrIS measured channel radiances X with a dimension $n \times t$, B is the prediction coefficient matrix with a dimension $m \times (n+1)$, and U is the $m \times t$ residual matrix. \times in (7) and also the following equations represents the matrix manipulation. The prediction coefficient matrix B then can be calculated through (8) with the training data set

$$B = (D_X^T \times D_X)^{-1} \times D_X^T \times Y \quad (8)$$

where T and the superscript -1 represent the transpose and inverse, respectively. However, due to the multicollinear problem as mentioned before, B cannot be directly calculated using (8).

To solve this issue, a principal component transformation is performed on X through (9), to decorrelate the measured channel radiances into orthogonal principal component scores pcs_X before deriving the coefficients

$$pcs_X = (X - \bar{X}) \times N_X^{-1} \times E_X^T \quad (9)$$

where N_X and \bar{X} are the instrument noises and mean radiances of the measured channels of the training data set, respectively. E_X are the eigenvectors decomposed from the following equation

$$S_X = E_X \times \Lambda_X \times E_X^T \quad (10)$$

where S_X is the covariance matrix of the noise normalized radiances and Λ_X is the diagonal eigenvalue matrix. The noise normalization will make the channel noise approximately white and greatly enhances the signal to noise ratio throughout the whole spectrum when calculating the eigenvectors [16].

Thus, by replacing X in the design matrix with pcs_X , the relationship between the principal component scores of the measured channel radiances and the gap channel radiances now can be properly established through (11) with the training data set

$$B_{\text{pcs}} = (D_{\text{pcs}_X}^T \times D_{\text{pcs}_X})^{-1} \times D_{\text{pcs}_X}^T \times Y \quad (11)$$

where the B_{pcs} is the principal components-based gap channel prediction coefficient matrix. Since most of the earth spectral variances are mainly distributed in the first few principal components, only the leading k_X principal component scores are used as the predictors. By using only the leading principal components, (11) becomes

$$B_{\text{pcs}} = (D_{\text{pcs}_X}'^T \times D_{\text{pcs}_X}')^{-1} \times D_{\text{pcs}_X}'^T \times Y \quad (12)$$

where D_{pcs_X}' is the design matrix after the matrix D_{pcs_X} is truncated by retaining only the first few vectors (hereafter, the symbol ' indicates the truncated matrix or its result is truncated).

The gap channel radiances of the training data set Y used in (11) and (12) still have significant amounts of instrument noise. Therefore, it is necessary to reduce the noise to get better regression accuracy. To obtain the noise-decreased gap channel radiances represented by Y_{dec} , the principal component scores pcs_Y of Y are first calculated by using the same equations that are applied to the measured channels (by replacing X in (9) and (10) with Y). Only the leading k_Y principal component scores pcs_Y' are retained and transformed back with (13) to get the noise-decreased gap channel radiances

$$Y_{\text{dec}} = pcs_Y' \times E_Y' \times N_Y + \bar{Y} \quad (13)$$

where similarly, N_Y and \bar{Y} are the instrument noises and mean radiances of the gap channels, respectively, and E_Y' contains the eigenvectors decomposed from the covariance of the corresponding gap channel radiances.

Eventually, based on the optimized predictors and response variables, the prediction coefficient matrix B_{pcs} can be successfully regressed with training data set by using

$$B_{\text{pcs}} = (D_{\text{pcs}_X}'^T \times D_{\text{pcs}_X}')^{-1} \times D_{\text{pcs}_X}'^T \times Y_{\text{dec}}. \quad (14)$$

In (14), the B_{pcs} is a $m \times (k_X + 1)$ matrix with the first row is the constant variable and the rest of rows are the coefficients. The number of principal components to retain is determined by the square root of decomposed eigenvalues (SRE). The principal components are retained until the SRE has no obvious changes, since then the noise will gradually become dominant in the rest of the principal components. The number of principal components k_X that used as predictors in this paper is 110. While the noise-decreased LW, MW, and SW gap channel radiances in Y_{dec} are separately reconstructed from their first 20, 35, and 8 leading principal component scores of Y , respectively. Due to the solar reflectivity and sun glint in the SW band, only nighttime data are used in deriving the prediction coefficients of the SW gap channels. (Hereafter, only the nighttime data are used when dealing with SW gap channels.)

As explained in (9) and (10), the instrument channel noises of the full-CrIS training data set have to be used in the PCA for the purpose of data normalization. However, it is not easy to directly derive the channel noises of the full-CrIS from the original instrument noises of IASI. This is because the IASI instrument noises have been changed a lot after a series of mathematical operations like the apodization transformation and truncation during the spectral conversion.

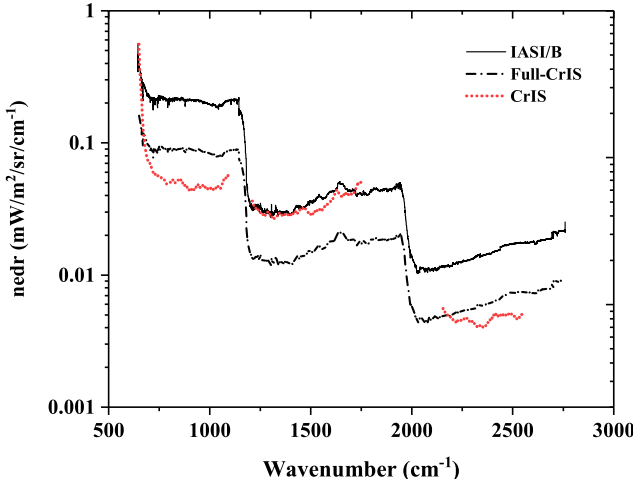


Fig. 3. IASI/B, IASI converted full-CrIS and the CrIS instrument noises. The noise of IASI/B is Gaussian apodized and obtained from its level 1 principal component compression product, which are averaged by all four FOVs. The noise of full-CrIS is estimated from IASI/B. The instrument noise of CrIS is hamming apodized and obtained from its SDR product with FOV averaged.

In this paper, the full-CrIS instrument noises are estimated from a set of theoretical simulated spectra. They are calculated by the Planck function with BT at 280 K. The IASI instrument noises are randomly and independently added to the each of the spectra. By using the identical conversion method, these simulated spectra with added IASI instrument noises are converted into full-CrIS resolution. The full-CrIS channel instrument noises are then estimated from the corresponding standard deviation of the converted full-CrIS channel radiances, as shown in Fig. 3.

In using this method, the measured channels of the real CrIS data X_{CrIS} need to be first projected onto the principal component space with parameters (mean, instrument noise, and eigenvectors) derived from the training data. This is because the prediction coefficient matrix is derived based on the principal components scores instead of the original measured channel radiances. Finally, the CrIS gap channel radiances in Y_{CrIS} are predicted from the real CrIS data through

$$Y_{\text{CrIS}} = [(X_{\text{CrIS}} - \bar{X}) \times N_X^{-1} \times E_X^T]' \times P_{\text{pcs}} + C_{\text{pcs}}^T \quad (15)$$

where C_{pcs} is the constant row of the B_{pcs} and P_{pcs} is the coefficient rows of the B_{pcs} .

Since the instrument noise of the real CrIS is not identical to the IASI simulated full-CrIS (Fig. 3), extra noise is probably induced into the predictors if the real CrIS data are transformed into the principal component space with parameters derived from full-CrIS training data set. Some of the CrIS channel noises will be enhanced in (15) if they were higher than those of the full-CrIS, and vice versa. A better way to solve this issue is to apply a PCA noise filter to the real CrIS data before it is transformed onto the principal component space with the parameters derived from the full-CrIS. This will greatly reduce the noise of the real CrIS data and possibly make the overall noise lower than the full-CrIS training data set. This is particularly useful when the proposed method is applied to other instruments which have a higher or totally

different noise from the training data set. However, since the CrIS instrument noises is overall similar to that of the full-CrIS and only the first few leading principal components are used as the predictors, the CrIS noises left in the predictors is basically very small. Therefore, the uncertainties caused by the difference of instrument noises between real CrIS and full-CrIS should be neglected.

III. VALIDATION

A. Fitting Accuracy Analysis

The evaluation of the prediction results is challenging because we do not have real measured data in these CrIS gap channels. Thus, we first present a validation method to theoretically analyze the accuracy of the CrIS gap channel prediction results. One day of IASI/B data with 1 265 674 total observations (after the negative spectra were removed) on October 30, 2016, which are not included in the training data set, are selected and simulated into full-CrIS spectra by using the IASI to CrIS conversion method. Note that in this fitting error analysis, the real CrIS measurements are not involved. In other words, the measured channels in X are also obtained from the full-CrIS spectra. The gap channel radiances in Y_P are first predicted from the measured channels in X , and then Y_P is compared to Y which contains the corresponding channels in the full-CrIS spectra after the noise was filtered with previous derived principal component parameters. Since Y (from IASI measurements) can be regarded as a truth value, the overall fitting accuracy of the proposed prediction method can be estimated by comparing the radiances between Y_P and Y .

Fig. 4(a) and (b) shows the BT differences between the predicted and the directly converted CrIS gap channel radiances in kelvin based on one day's global data. Theoretically, the uncertainties are mainly contributed from the regression if the training data set is well representative for different atmospheric and surface conditions. As shown, the mean bias in the LW gap spectral region is very small within ± 0.005 K, while in the MW gap spectral region it is distributed between ± 0.06 K. The standard deviations of their channel differences are generally less than 0.2 and 0.5 K in the LW and MW gap spectral regions, respectively. Their differences in the SW are a little bit larger than those observed in LW and MW. The mean biases are less than 0.05 K and standard deviations are less than 1 K for most of the SW channels. Considering the total number of observations, the prediction uncertainties on the mean bias (standard error) are around 0.18, 0.45, and 0.71 mK over the LW, MW, and SW spectral gap regions, respectively. One interesting feature in Fig. 4(b) is that their standard deviation tends to show an increasing pattern along with the increase of wavenumber. This is because the fitting method is in the radiance space and same bias in radiance value will give much larger BT difference in the SW band than in the LW band due to the nature of Planck function. The mean biases are basically caused by the linear assumption between the CrIS measured and gap channels, which will induce small bias in practice. This is because their relationships are nonlinear. Overall, the predicted values agree

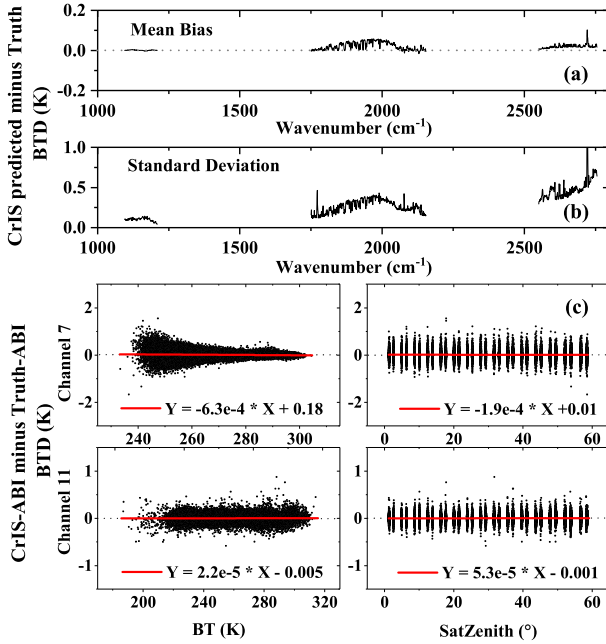


Fig. 4. BT (a) mean bias and (b) standard deviation between the predicted and truth gap channel values based on one day's IASI/B converted full-CrIS data on October 30, 2016. (c) Scene and scan angle dependent between the simulated CrIS-ABI (without gap) and truth-ABI over channel 7 (central wavenumber is 2570.37 cm^{-1}) and 11 (central wavenumber is 1184.22 cm^{-1}). Overlapped points are not shown in (c) due to too many points, but the analysis is based on all of the data.

well with the supposed truth even though jumps are observed in some of the MW and SW gap channels, such as the channels around 1772.5 and 2720 cm^{-1} . Therefore, it suggests that most of the CrIS gap channel information can be successfully derived from its measured channels by using the proposed method. We should point out that, the predicted channel radiances are intended to be only used in the intercomparison proposes instead of providing exact information of these gap channels.

In addition, to see if there is any scene or scan angle dependencies of the predicted gap radiances, a further investigation is conducted based on the simulated CrIS-ABI data. Firstly, the abovementioned IASI/B converted full-CrIS spectra are convolved with the SRF of GOES-16 ABI channel 7 and 11 using (16) to obtain the full-CrIS simulated ABI data

$$R_{\text{CrIS-simulated}} = \frac{\int_{v1}^{v2} R_{\text{CrIS}}(v) \cdot S(v) \cdot dv}{\int_{v1}^{v2} S(v) \cdot dv} \quad (16)$$

where R_{CrIS} is the CrIS channel radiances, $v1$ and $v2$ are the spectral wavenumber range of the broadband channel, and S is the interpolated broadband channel SRF, the $R_{\text{CrIS-simulated}}$ is the CrIS simulated broadband channel radiance. The full-CrIS simulated ABI spectra then can be regarded as the truth values (refer to truth ABI). Secondly, the CrIS measured channels are extracted from the full-CrIS spectra and are used to predict out the gap channel radiances by using the proposed method. Then, the measured channels along with their predicted gap channels are also convolved with the SRF of GOES-16 ABI channels using (16) to obtain the CrIS simulated ABI data (refer to CrIS-ABI) after the spectral gaps were filled. At last,

their scene and scan angle dependencies are shown in Fig. 4(c). As the red regression line shown, scan angle dependence is hardly found between CrIS and ABI over the two spectral gap channels, which suggests that the training data set is not sensitive to scan angle, and thus it is not necessary to separate with different scan angles. The off-nadir observations basically have similar gap filling accuracies with those of the nadir observations. In addition, there is no strong scene dependent feature too over the two selected channels. However, larger differences with a slightly positive bias should be expected between them in the very cold scenes. This is because the IASI SW observations are supposed to have larger noises over the very cold scenes with many channel radiances are negative, and these noises cannot be fit by any regression method.

B. Intercomparison With Hyper-Spectral Infrared Sounders

Intercomparison between CrIS and other hyper-spectral infrared sounders based on the simultaneous nadir overpass (SNO) events provide another way to evaluate the accuracy of the predicted gap channel radiances. AIRS basically has the same local equatorial crossing time with CrIS but with different altitudes. This provides opportunities for us to compare CrIS to AIRS in both the measured and predicted channels at different latitudes. The CrIS-IASI SNO events usually occur between 70° and 80° of the North and South Polar Regions within a few seconds at nadir view, since their satellites have different altitudes and local equatorial crossing time. For each of the AIRS, IASI/A, and IASI/B instruments, four days SNO observed data are used in the intercomparison between CrIS and them. The initial SNO points used are from NOAA National Calibration Center (<https://ncc.nesdis.noaa.gov/SNOPredictions/>). The CrIS nadir (FOR 15 and 16) homogenous SNO data are then extracted for each of these SNO events by using a series of selection criteria, such as FOV distance, and time difference. In particular, the VIIRS pixels within the CrIS FOV are used to check the CrIS-AIRS/IASI collocated scene homogeneity by examining the standard deviation to the mean ratio of the VIIRS band M16 radiances. The CrIS-VIIRS collocation method used in this paper is the same as [25]. Detailed information for the selected CrIS-AIRS and CrIS-IASI SNO events are summarized in Table II.

1) *CrIS Versus AIRS*: The direct comparison between CrIS and AIRS is a challenge because CrIS is Michelson interferometer with uniform channel response function, while AIRS is a grating spectrometer with channel center frequencies and individually tabulated SRFs. Therefore, the key issue in the comparison is how to translate the spectral resolution varied AIRS channels to the equal spectral interval channels of CrIS. In this paper, we use the method proposed by Motteler [26]. The first step in the AIRS to CrIS conversion is to deconvolve the AIRS channel radiances to an intermediate spectrum with equal spectral resolution. Suppose the AIRS channel radiances Y_{AIRS} are measured by convolving the TOA monochromatic spectrum X_{TOP} with a very fine monochromatically tabulated channel SRF matrix F

$$Y_{\text{AIRS}} = F \times X_{\text{TOP}}. \quad (17)$$

TABLE II
SNO DATA COLLOCATION CRITERIA FOR CRIS–AIRS AND CRIS–IASI

Condition	AIRS		
	High-latitude	Low-latitude	IASI A/B
FOV distance (Separation of FOV centers)	less than 6.875 km	less than 6.5 km	
Time difference	less than 2 min	less than 15 min	less than 2 min
FOR index	Only CrIS FOR 15 and 16 data are used	A: 13, 14 August and 3, 4 October 2016	
SNO date	10, 13, 16, 18 November 2016	B: 9, 10 September, 31 October, and 1 November 2016	
FOV homogeneity	VIIRS M16: stddev(M16) / mean(M16) less than 0.05		

Theoretically, the TOA radiances can be deconvolved by calculating the pseudoinverse of F

$$Y_{\text{TOA}} = F^{-1} \times Y_{\text{AIRS}} \quad (18)$$

where F^{-1} is the pseudoinverse matrix of F . However, in practice, there are problems. The calculation of the F^{-1} will become unstable if the channel SRF matrix is too large. To solve this problem, a compromised intermediate spectrum is deconvolved from AIRS channel radiances. This is done by calculating the pseudoinverse of an approximate AIRS channel SRF matrix with an equal spectral resolution of 0.1 cm^{-1} . This approximate matrix is more manageable in calculating its pseudoinverse, even though it will lose some information on this approximation. After that, the intermediate spectrum is converted into CrIS by using the identical IASI-CrIS conversion method detailed in Section II.

The intercomparison between CrIS and AIRS is performed only around the LW gap spectral region. This is because the AIRS does not cover the MW gap channels of CrIS and its SW channels basically have a lower spectral resolution than the FSR mode CrIS. The conversion residual between CrIS and AIRS converted CrIS is generally less than 0.1 K in the LW [26], which can be negligible in the intercomparison study. As shown in Fig. 5, the predicted CrIS gap spectra (the shadow region in Fig. 5) agree well with those observed by AIRS (hereafter refers to AIRS converted CrIS) both in the polar and the tropical regions. Their BT differences are close to zero with a standard deviation of less than 1 K for all the selected earth scenes. Moreover, the BT differences observed over the predicted channels is similar to those of the measured channels (less than 1095 cm^{-1} and greater than 1210 cm^{-1}) both in mean and standard deviation. The consistent results between CrIS and AIRS imply that the predicted CrIS LW gap channels are accurate enough to be used in the intercomparison studies. In fact, it is not surprising to see the good performance of the proposed gap-filling method in the LW spectral gap region. This is because the LW gap channels are within the atmospheric window region and do not contain many atmospheric absorption lines.

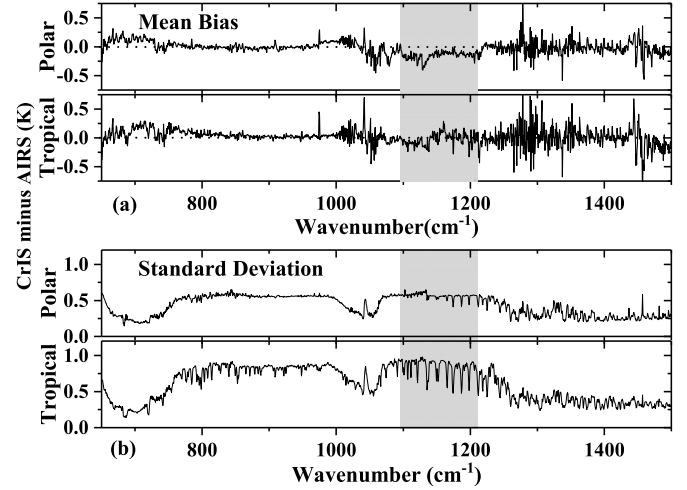


Fig. 5. Intercomparison results of (a) mean bias and (b) standard deviation between CrIS and AIRS converted CrIS in the polar and tropical regions based on four days (November 10, 13, 16, and 18, 2016) SNO events. The shadow area shows the CrIS spectral gap regions.

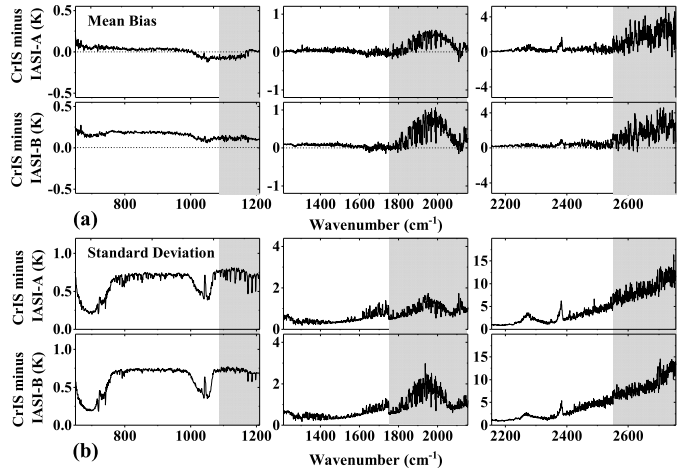


Fig. 6. Intercomparison results of (a) mean bias and (b) standard deviation between CrIS and IASI/A/IASI/B converted CrIS based on four days (IASI/A: August 13 and 14, 2016 and October 3 and 4, 2016 and IASI/B: September 9 and 10, 2016, October 31, 2016, and November 1, 2016) SNO events. The shadow areas indicate the CrIS spectral gap regions.

2) *CrIS Versus IASI*: The intercomparison between CrIS and IASI is performed by converting IASI spectra to CrIS through the method described in Section II. Fig. 6 shows the comparison results of CrIS–IASI/A and CrIS–IASI/B from 650 to 2755 cm^{-1} . As shown, good agreements are observed between CrIS and IASI in the LW region. At the LW gap spectral region, their BT differences are very small with a mean bias of 0.1 K and a standard deviation of less than 1 K for both the CrIS–IASI/A and CrIS–IASI/B, which is very similar to the results observed from the CrIS–AIRS SNO events.

At the edge channels in MW water vapor absorption gap spectral region, consistent results are also observed between CrIS and IASI. The mean biases are around 0.1 K and standard deviations are mostly less than 1 K . However, the uncertainties in the other MW gap channels are larger than those of LW gap

channels, especially in the spectral region between 1900 and 2000 cm⁻¹. The mean BT differences of CrIS–IASI/A and CrIS–IASI/B in these channels are generally around 0.5 K and their standard deviations are changed from 1 to 3 K dependent on the specific spectral absorption regions. This phenomenon implies that CrIS currently measured spectral information is insufficient to retrieval all the gap channel information in the MW band. Some special absorption lines may only exist in these channels, making them hard to be predicted by other channels. For intercalibration with other narrow- or broadband instruments, relatively larger bias and standard deviation should be expected at these regions.

At the SW gap region, both of the BT differences and the standard deviation are significantly increased through the comparison with the LW and MW regions. Their spectral means are generally less than 3 K and standard deviations can reach as high as 10 K along with the increase of wavenumber. Since the radiances in the SW channels are much smaller than those in the other two spectral regions, it is reasonable see larger BT differences between CrIS and IASI in the SW spectral region. Another explanation of the large uncertainties is probably due to the decreasing radiance value in the SW band for cold scenes, since the SNO scenes are selected only from Polar Regions and the nighttime. As mentioned before, both CrIS and IASI observations have larger noises over cold scenes. Even though, when examining their BT differences, no considerable sharp increase can be found in the predicted SW gap channels. As seen in Fig. 6, the BT uncertainties in SW band are smoothly increased from the measured to the predicted channels with the increase of wavenumber. This implies that most of the SW gap channels can also be correctly predicted.

In general, the predicted CrIS gap spectra agree well with those measured by other hyper-spectral sounders except for some absorption channels. The good consistency generally implies that the predicted CrIS gap channel radiances can be used for intercalibration of broadband sensors.

IV. APPLICATION

With the results from this paper, CrIS now can be used as a reference to compare with broadband channels that fall within these gaps. To demonstrate the new CrIS capability, the SNPP VIIRS M14, GOES-16 ABI channels 7, 8, and 11 are used to show the performance of the proposed spectral gap prediction method. Before doing the comparison, the global CrIS–VIIRS and CrIS–ABI data are paired together. Then, the CrIS spectra are simulated into broadband radiances by using (16) and compared with spatially averaged broadband channel radiances within each of the CrIS FOVs. To keep consistence, the CrIS minus other broad instruments are used in this paper. However, we must mention that when using CrIS as a reference instrument, it would be more conventional to show the comparison of broad instrument minus CrIS.

A. CrIS and VIIRS

As shown in Fig. 1 and Table I, it is impossible to use original CrIS measurements to evaluate the accuracy of the

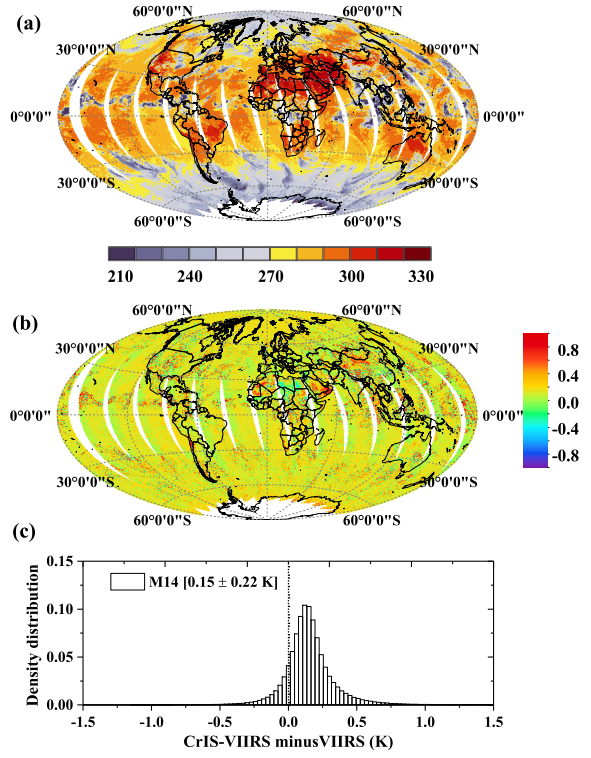


Fig. 7. Spatial maps of (a) VIIRS M14 BT and (b) its difference (CrIS minus VIIRS) with CrIS simulated VIIRS (only ascending data are shown), and (c) density distribution maps of their BT difference. The data used for the comparison are selected from on August 5, 2017.

VIIRS channel M14 due to the huge gap of CrIS in this spectral region. By using the proposed spectral gap prediction method, the intercomparison work can now be performed between CrIS and VIIRS channel M14. Fig. 7 shows the global BT differences between VIIRS and CrIS simulated VIIRS at channel M14 on August 5, 2017. As shown, the spectral gap prediction method works very well for the VIIRS channel M14. Most of their BT differences are less than 0.2 K [Fig. 7(b)], with a global mean of 0.15 and standard deviation of 0.22 K [Fig. 7(c)] for all the homogeneous and inhomogeneous earth scenes. In addition, their BT differences also show weak scene dependent pattern which is consistent with patterns observed over channels M15 and M16 in [27].

The CrIS and VIIRS daily data is further analyzed based on the homogeneous scenes (the standard deviation to mean ratio of the VIIRS M16 radiances within CrIS FOV less than 0.01) during the period from October 2017 to November 2017. In addition to channel M14, the differences at channels M15 and M16 are also investigated. As shown in Fig. 8, consistent results are clearly observed for their daily mean and standard deviation (black curve) over M14 as well as the other two channels. The slope of linear regression (red curve) is very small albeit statistically significant, indicating that the proposed spectral gap-filling method is very stable. However, since the original CrIS spectrum only covers 0.01% of the VIIRS M14 SRF, both the mean bias and standard deviation between these two sensors are a little higher than those from channels M15 and M16. The spectral coverage is calculated by dividing the total channel SRF with that of covered only

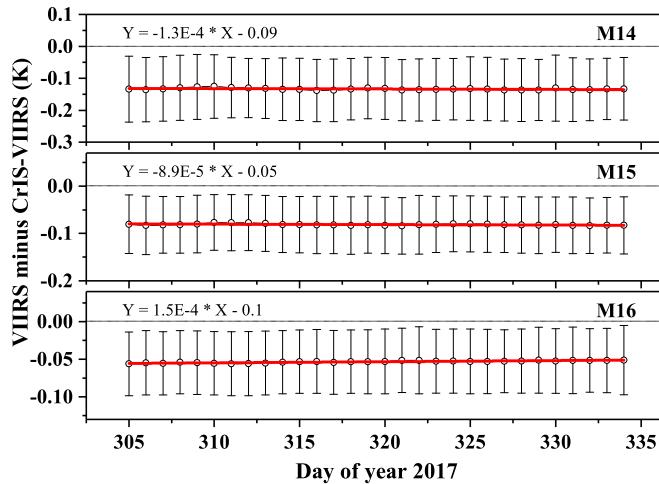


Fig. 8. Daily BT differences between VIIRS and CrIS (without gap) simulated VIIRS at channels M14, M15, and M16. The black curves are their daily mean bias with standard deviation plotted as error bar, while the red curves are their linear fitting line. As shown, stable results are observed between CrIS after gap was filled and VIIRS M14.

by CrIS spectrum. Nevertheless, the time series result still indicates that the predicted CrIS LW gap channels are reliable and can be used as a good reference in intercalibration.

B. CrIS and ABI

Similarly, the original spectrum of CrIS covers only about 10% of the ABI channel 11, while its coverage in SW band for the ABI channel 7 is around 30%. In addition, nearly 0.3% of the spectral coverage is still missing when comparing CrIS with ABI at the water vapor channel 8. To see the capability of CrIS without gap as a reference over these channels, SNO data that selected from approximate nadir and homogenous (the standard deviation to the mean ratio of the ABI channel 14 radiances within CrIS FOV are used to check the homogeneity) scenes were investigated during the period from October 2017 to December 2017. Furthermore, to facilitate the analysis, the intercomparisons between ABI and IASI/A and B over these three channels were also conducted in the same period. Detailed SNO selection criteria for the CrIS–ABI and IASI–ABI are in Table III. We have to point out that when use Low Earth Orbit (LEO) hyper-spectral infrared sounder as a reference to check the calibration accuracy of the Geostationary Earth Orbit (GEO) broadband instruments, it is better to include all the paired scenes instead of only the homogeneous scenes in practice, such as the research conducted by Hewison *et al.* [28], the inverse of the variance of the GEO satellite radiances within each LEO hyper-spectral satellite FOV is used as the weighting to represent the uncertainty in the collocation due to spatial variability.

As shown in Fig. 9, the comparisons between CrIS and ABI over huge gap channels of 7 and 11 show stable and very promising results. Both the mean bias and standard deviation are in the same uncertainty level with those observed from IASI/A and IASI/B. This indicates that the prediction uncertainty of the proposed method is far lower than the

TABLE III
SNO DATA COLLOCATION CRITERIA FOR CRIS–ABI AND IASI–ABI

Condition	CrIS	IASI A/B
FOV distance (Separation of FOV centers)	less than 6.875 km	less than 6.5 km
Time difference		less than 10 min
FOR index	from 14 to 17	from 13 to 18
View angle difference abs(cos(zenith1)-cos(zenith2))		less than 0.02
SNO date		October–December 2017
FOV homogeneity	ABI channel 14: stddev(ch14) / mean(ch14) less than 0.01	

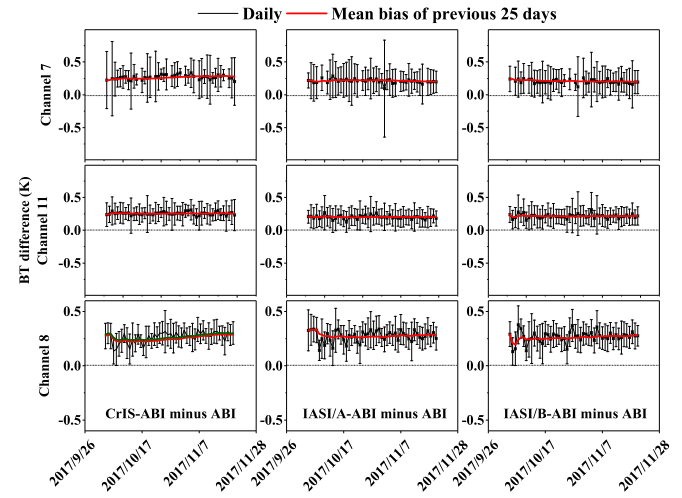


Fig. 9. Time series BT differences between ABI and hyper-spectral sounders (CrIS without gap, IASI/A, and IASI/B) simulated ABI at channels 7, 8, and 11 (sounders minus ABI). Black curves are their daily mean bias with standard deviation plotted as error bar. Red curves are their mean bias calculated from previous 25 days. In particular, the green curve plotted in channel 8 is the previous 25 days' mean bias calculated between ABI and original CrIS spectra (has little gap in this channel) simulated ABI. As shown, the difference between CrIS without gap and ABI are comparable with those observed from IASI/A and IASI/B, and the mean bias of channel 8 has also been reduced after the little spectral gap is filled.

intercomparison uncertainty from sensor to sensor when the CrIS convolved with the broadband channels. Moreover, their mean bias also slightly decreased over the water vapor channel 8 after the little gap was filled by the method, as the green line (before the gap was filled) shows in Fig. 9.

In general, the global difference between CrIS and VIIRS M14 is comparable with those by CrIS fully covered VIIRS channels after the LW spectral gap is filled. Moreover, both the simulated CrIS and ABI intercomparison, and the joint intercomparison between real CrIS, IASI, and ABI over CrIS unmeasured spectral regions reveal that CrIS can reach to a similar intercomparison accuracy with IASI after its spectral gaps are filled. All these suggested that the predicted CrIS gap radiances indeed improve a lot on the intercomparison results between CrIS and broadband instruments over the spectral gap regions and can be confidently applied in GSICS community.

V. DISCUSSION AND CONCLUSION

The SNPP CrIS has spectral gaps among its measurements which significantly impact the intercomparison capability and accuracy between CrIS and other instruments. In this paper, a new spectral gap-filling method was developed to predict the CrIS gap channels based on the principal component-based regression method.

The fitting uncertainties of the predictions in the LW, MW, and SW gap spectral regions are basically very small. However, absorption line features are observed in some MW and SW gap channels, suggesting that the CrIS gap channel spectral information cannot be completely predicted from the current measured channels. The intercomparisons with other hyper-spectral sounders (AIRS and IASI/A/IASI/B) also show acceptable results, especially for the LW channels. Good consistency between CrIS and other hyper-spectral sounders suggest that the predicted CrIS gap channel radiances can be used by broadband sensors in intercalibration studies. The performance of CrIS when used as a reference in the intercalibration without spectral gaps is investigated by using SNPP VIIRS and GOES16 ABI as examples. Stable and promising results can be obtained between CrIS and other broadband channels that fall within the spectral gap regions, implying that the predicted CrIS gap channel radiances are good enough for the intercalibration comparison purpose under the GSICS framework.

Overall, the CrIS spectrum without gaps is needed in many fields. However, due to the hardware design of the instrument, spectral gaps will continual exist in the upcoming JPSS-1 and also the JPSS-2 CrIS. Therefore, how to accurately fill up these spectral gaps become essentially important now. Even though the proposed gap channel prediction method shows great potential in the intercalibration studies, more works still need to be done in the near future. For example, the training data set needs to be improved in further studies. Currently, the prediction coefficients are derived from IASI simulated CrIS training data set. However, small errors may be induced when applying them to the real CrIS measured data. As a reference infrared instrument, the intercomparison performance of the predicted CrIS gap channels with other geostationary sensors, such as AHI and the Advanced Geosynchronous Radiation Imager on board the recently launched FengYun-4 satellite also need to be further investigated in the future studies.

ACKNOWLEDGMENT

The authors would like to thank NOAA's Comprehensive Large Array Data Stewardship System, the NASA's Data and Information Services Center, and the EUMETSAT Data Center for providing the scientific satellite data. They would like to thank Dr. Y. Han, who has retired from the NOAA/NESDIS/Center for Satellite Applications and Research, for providing valuable suggestions and critic comments for this paper. They would also like to thank F. Yu for providing valuable comments for the study. The contents of this paper are solely the opinions of the authors and do not constitute a statement of policy, decision, or position on behalf of NOAA or the U.S. Government.

REFERENCES

- [1] Y. Han *et al.*, "Suomi NPP CrIS measurements, sensor data record algorithm, calibration and validation activities, and record data quality," *J. Geophys. Res., Atmos.*, vol. 118, no. 22, pp. 12734–12748, Nov. 2013, doi: [10.1002/2013JD020344](https://doi.org/10.1002/2013JD020344).
- [2] A. Gambacorta *et al.*, "An experiment using high spectral resolution CrIS measurements for atmospheric trace gases: Carbon monoxide retrieval impact study," *IEEE Geosci. Remote Sens. Lett.*, vol. 11, no. 9, pp. 1639–1643, Sep. 2014, doi: [10.1109/LGRS.2014.2303641](https://doi.org/10.1109/LGRS.2014.2303641).
- [3] A. Smith, N. Atkinson, W. Bell, and A. Doherty, "An initial assessment of observations from the Suomi-NPP satellite: Data from the Cross-track Infrared Sounder (CrIS)," *Atmos. Sci. Lett.*, vol. 16, no. 3, pp. 260–266, 2015, doi: [10.1002/asl2.551](https://doi.org/10.1002/asl2.551).
- [4] L. Lin, X. Zou, and F. Weng, "Combining CrIS double CO₂ bands for detecting clouds located in different layers of the atmosphere," *J. Geophys. Res., Atmos.*, vol. 122, no. 3, pp. 1811–1827, Feb. 2017, doi: [10.1002/2016JD025505](https://doi.org/10.1002/2016JD025505).
- [5] Y. Chen, Y. Han, and F. Weng, "Characterization of long-term stability of Suomi NPP Cross-track Infrared Sounder spectral calibration," *IEEE Trans. Geosci. Remote Sens.*, vol. 55, no. 2, pp. 1147–1159, Feb. 2017, doi: [10.1109/TGRS.2016.2620438](https://doi.org/10.1109/TGRS.2016.2620438).
- [6] L. Wang, Y. Han, D. Tremblay, F. Weng, and M. Goldberg, "Intercomparison of NPP/CrIS radiances with VIIRS, AIRS, and IASI: A post-launch calibration assessment," presented at the SPIE Asia-Pacific Remote Sens. Meeting, 2012. [Online]. Available: <https://www.spiedigitallibrary.org/conference-proceedings-of-spie/8528/1/Inter-comparison-of-NPP-CrIS-radiances-with-VIIRS-AIRS-and/10.1117/12.978769.short?SSO=1>
- [7] D. C. Tobin, H. Revercomb, R. Knuteson, J. Taylor, and D. Deslover, "Cal/Val of CrIS on Suomi-NPP: Intercalibration with AIRS, IASI, and VIIRS," presented at the 9th Annu. Symp. Future Oper. Environ. Satell. Syst. Meeting, 2013. [Online]. Available: <https://ams.confex.com/ams/93Annual/webprogram/Paper224176.html>
- [8] Y. Li, A. Wu, and X. Xiong, "Inter-comparison of S-NPP VIIRS and Aqua MODIS thermal emissive bands using hyperspectral infrared sounder measurements as a transfer reference," *Remote Sens.*, vol. 8, no. 1, p. 72, Nov. 2016, doi: [10.3390/rs8010072](https://doi.org/10.3390/rs8010072).
- [9] D. C. Tobin, H. E. Revercomb, C. C. Moeller, and T. S. Pagano, "Use of Atmospheric Infrared Sounder high-spectral resolution spectra to assess the calibration of Moderate Resolution Imaging Spectroradiometer on EOS Aqua," *J. Geophys. Res. Atmos.*, vol. 111, p. D09S05, May 2006, doi: [10.1029/2005JD006095](https://doi.org/10.1029/2005JD006095).
- [10] P. Veglio, D. C. Tobin, S. Dutcher, G. Quinn, and C. C. Moeller, "Long-term assessment of Aqua MODIS radiance observation using comparisons with AIRS and IASI," *J. Geophys. Res., Atmos.*, vol. 121, no. 14, pp. 8460–8471, Jul. 2016, doi: [10.1002/2015JD024653](https://doi.org/10.1002/2015JD024653).
- [11] M. M. Gunshor, T. J. Schmit, W. P. Menzel, and D. C. Tobin, "Intercalibration of broadband geostationary imagers using AIRS," *J. Atmos. Ocean. Technol.*, vol. 26, no. 4, pp. 746–758, Apr. 2009, doi: [10.1175/2008JTECHA1155.1](https://doi.org/10.1175/2008JTECHA1155.1).
- [12] Y. Tahara and K. Kato, "New spectral compensation method for intercalibration using high spectral resolution sounder," Meteorol. Satell. Center, Japan Meteorol. Agency, Tokyo, Japan, Tech. Rep. 52, Feb. 2009, pp. 1–37.
- [13] M. Goldberg *et al.*, "The global space-based inter-calibration system," *Bull. Amer. Meteorol. Soc.*, vol. 92, no. 4, pp. 467–475, Apr. 2011, doi: [10.1175/2010BAMS2967.1](https://doi.org/10.1175/2010BAMS2967.1).
- [14] I. T. Jolliffe, "A note on the use of principal components in regression," *J. Roy. Stat. Soc.*, vol. 31, no. 3, pp. 300–303, Jun. 1982, doi: [10.2307/2348005](https://doi.org/10.2307/2348005).
- [15] E. Bair, T. Hastie, D. Paul, and R. Tibshirani, "Prediction by supervised principal components," *J. Amer. Stat. Assoc.*, vol. 101, no. 473, pp. 119–137, 2006, doi: [10.1198/016214505000000628](https://doi.org/10.1198/016214505000000628).
- [16] P. Antonelli *et al.*, "A principal component noise filter for high spectral resolution infrared measurements," *J. Geophys. Res., Atmos.*, vol. 109, p. D23102, Dec. 2004, doi: [10.1029/2004JD004862](https://doi.org/10.1029/2004JD004862).
- [17] Y. Han and Y. Chen, "Calibration algorithm for Cross-track Infrared Sounder full spectral resolution measurements," *IEEE Trans. Geosci. Remote Sens.*, vol. 56, no. 2, pp. 1008–1016, Feb. 2018, doi: [10.1109/TGRS.2017.2757940](https://doi.org/10.1109/TGRS.2017.2757940).
- [18] M. T. Chahine *et al.*, "AIRS: Improving weather forecasting and providing new data on greenhouse gases," *Bull. Amer. Meteorol. Soc.*, vol. 87, no. 7, pp. 911–926, Jul. 2006, doi: [10.1175/BAMS-87-7-911](https://doi.org/10.1175/BAMS-87-7-911).

- [19] AIRS Science Team/Moustafa Chahine, "AIRS/Aqua L1C Infrared (IR) resampled and corrected radiances V006," 2015. Distributed by Goddard Earth Sciences Data and Information Services Center, Greenbelt, MD, USA, doi: [10.5067/Aqua/AIRS/DATA101](https://doi.org/10.5067/Aqua/AIRS/DATA101).
- [20] F. Hilton *et al.*, "Hyperspectral earth observation from IASI: Five years of accomplishments," *Bull. Amer. Meteorol. Soc.*, vol. 93, pp. 347–370, Mar. 2012, doi: [10.1175/bams-d-11-00027.1](https://doi.org/10.1175/bams-d-11-00027.1).
- [21] C. Cao *et al.*, "Suomi NPP VIIRS sensor data record verification, validation, and long-term performance monitoring," *J. Geophys. Res., Atmos.*, vol. 118, no. 11, pp. 11664–11678, Oct. 2013, doi: [10.1002/2013JD020418](https://doi.org/10.1002/2013JD020418).
- [22] L. Wang *et al.*, "Geolocation assessment for CrIS sensor data records," *J. Geophys. Res., Atmos.*, vol. 118, no. 22, pp. 12690–12704, 2013, doi: [10.1002/2013JD020376](https://doi.org/10.1002/2013JD020376).
- [23] L. L. Strow *et al.*, "Spectral calibration and validation of the Cross-track Infrared Sounder on the Suomi NPP satellite," *J. Geophys. Res., Atmos.*, vol. 118, no. 22, pp. 12486–12496, Nov. 2013, doi: [10.1002/2013JD020480](https://doi.org/10.1002/2013JD020480).
- [24] L. Wang, Y. Han, Y. Chen, and D. A. Tremblay, "Radiometric consistency assessment of hyperspectral infrared sounders," *Atmos. Meas. Tech.*, vol. 8, no. 11, pp. 4831–4844, Nov. 2015, doi: [10.5194/amt-8-4831-2015](https://doi.org/10.5194/amt-8-4831-2015).
- [25] L. Wang, D. Tremblay, B. Zhang, and Y. Han, "Fast and accurate collocation of the Visible Infrared Imaging Radiometer Suite measurements with Cross-track Infrared Sounder," *Remote Sens.*, vol. 8, no. 1, p. 76, Jan. 2016, doi: [10.3390/rs8010076](https://doi.org/10.3390/rs8010076).
- [26] H. Motteler, (Jan. 29, 2016). *Deconvolution and Translation Between High Spectral Resolution IR Sounders*. [Online]. Available: https://github.com/strow/iasi_decon/blob/master/doc/decon_atbd.pdf
- [27] L. Wang, B. Zhang, D. Tremblay, and Y. Han, "Improved scheme for Cross-track Infrared Sounder geolocation assessment and optimization," *J. Geophys. Res., Atmos.*, vol. 122, no. 1, pp. 519–536, 2017, doi: [10.1002/2016JD025812](https://doi.org/10.1002/2016JD025812).
- [28] T. J. Hewison *et al.*, "GSICS inter-calibration of infrared channels of geostationary imagers using Metop/IASI," *IEEE Trans. Geosci. Remote Sens.*, vol. 51, no. 3, pp. 1160–1170, Mar. 2013, doi: [10.1109/TGRS.2013.2238544](https://doi.org/10.1109/TGRS.2013.2238544).



Hui Xu received the B.Sc. degree in computer science and technology and the M.Eng. degree in spatial data processing and analysis from Henan University, Kaifeng, China, in 2007 and 2010, respectively, and the Ph.D. degree in signal and information processing from the Institute of Remote Sensing and Digital Earth (RADI), Chinese Academy of Sciences, Beijing, China, in 2013.

He works as a Research Assistant and later an Associate Research Scientist at RADI from 2013 to 2017. He is currently a Post-Doctoral Research

Associate with the Earth System Science Interdisciplinary Research Center, University of Maryland, College Park, MD, USA, where he involved in the calibration and validation of satellite hyper-spectral infrared sounder.



Yong Chen received the B.S. and M.S. degrees in atmospheric sciences from Peking University, Beijing, China, in 1996 and 1999, respectively, and the Ph.D. degree in atmospheric sciences from the University of California, Los Angeles, CA, USA, in 2005.

From 2006 to 2013, he was a Research Scientist with the Cooperative Institute for Research in the Atmosphere, Colorado State University, Fort Collins, CO, USA. Since 2013, he has been a Research Scientist with the Earth System Science Interdisciplinary Research Center, University of Maryland, College Park, MD, USA. His research interests include radiative transfer theory and applications, development and implementation of fast radiative transfer model for satellite data assimilation, and radiometric and spectral calibration and validation of satellite hyper-spectral infrared sounder.



Likun Wang received the B.S. degree in atmospheric sciences and the M.S. degree in meteorology from Peking University, Beijing, China, in 1996 and 1999, respectively, and the Ph.D. degree in atmospheric sciences from the University of Alaska Fairbanks, Fairbanks, AK, USA, in 2004.

He was a Post-Doctoral Research Associate of lidar/radar remote sensing of clouds with the University of Maryland, College Park, MD, USA, from 2004 to 2005. He currently is an

Associate Research Scientist with the Earth System Science Interdisciplinary Research Center/Cooperative Institute for Climate Studies, College Park, MD, USA, in support of satellite sensor calibration and validation program for NOAA/NESDIS/STAR. With more than 12 years of progressive working experiences of NOAA's satellite sensors (e.g., hyper-spectral infrared sounder—cross-track infrared sounder (CrIS) and other infrared sounders—HIRS and SSU) and as research and project management roles, he is responsible for the pre- and postlaunch calibration testing data analysis, intercalibration for postlaunch instrument monitoring and assessment, ground processing software development, configuration and calibration parameter refining, and new algorithm design and integration.

Dr. Wang currently serves as a Lead for geometric calibration in the CrIS SDR Team and the Chair of World Meteorological Organization sponsored global space-based intercalibration system infrared sensor working group.